Journal of Engineering Sciences
Vol11,Issue2,FEB/2020
ISSN NO:0377-9254

Advanced Computational Methods versus Analytical and Empirical Solutions for Determining Restraint Stresses in Bottom-Restrained Walls

Janjirala kiran kumar
Department of Civil Engineering
Samskruti College of Engg & Tech
janjiralakiran123@gmail.com

Embadi harish
Department of Civil Engineering
Samskruti College of Engg & Tech
embadi.harish1000@gmail.com

Abstract

The distribution of restraint stresses in bottom-restrained walls is important information for the efficient crack con- trol of wall-like concrete members. Practical examples are retaining walls, bridge abutment walls or tank walls, for which the results can be used in order to assess the risk and intensity of harmful separating cracks over the wall height. Different solutions exist for the determination of these stress distributions, ranging from advanced computational methods over analytical and semi-analytical solutions up to empirical approaches. The aim of the present contribution is two- fold. On the one hand, the general applicability as well as commonalities and differences of the investigated solutions were demonstrated by using them for the analysis of a given demonstration example. On the other hand, a parametric study was carried out in order to assess the dependence of the prediction quality of the applied solutions on changing conditions. Altogether it was found that advanced computational methods and analytical or semi- analytical solutions showed a good agreement for common design tasks. Solutions with empirical modifications, however, were proved to be less satisfying from engineering perspective due to predefined parameters or mechanically inconsistent modifications.

1. Introduction

A wall-like concrete member is a concrete member with a pronounced length and height compared to its width. As soon as the deformation behaviour of such a wall-like member is restrained at the bottom, e.g. because they are cast on a foundation or slab, a distinct stress distribution from imposed thermal and moisture induced deformations occurs over the width, length and height of the wall. Main parameters on the size and shape of these stress distributions are the imposed deformation in the wall, stiffness ratios between wall and foundation (axial and bending stiffness) as well as length to height- ratio of the wall (L/H).

Practical examples, in which these restraint stresses are often relevant for the design of the minimum reinforcement are retaining walls, bridge abutment walls or tank walls. In particular, the appropriate determination of restraint stresses is needed to enable the reliable assessment of the cracking risk and crack width control, starting from hardening-induced stressing due to cement-hydration up to long-term behaviour throughout the whole service life of the structural member. Moreover, the appropriate quantification of restraint stresses is essential for new design concepts on basis of the deformation compatibility e.g. (BAW Bulletin 2011; Schlicke and Tue 2014; ÖBV Bulletin 2018). Currently available solutions for the determination of these restraint stresses range from advanced computational methods Advanced computa- tional methods are mainly used in science or for rather complex design tasks, whereas standard tasks in practice are preferably designed with analytical or semi- analytical solutions. The approaches given in guidelines and regulations are primarily based on analytical and semi-analytical solutions which are sometimes com- bined with empiricism, in order to represent the practi- cal observation accordingly.

A detailed investigation on the influences of common simplifications in analytical and semi-analytical solutions was already presented in (Schlicke *et al.* 2018). Another common discussion point is the comparability of the results of advanced computational methods with the ones of analytical or semi-analytical solutions. Therefore, a demonstration example was predefined and investigated with different methods. Discussed are namely, a thermomechanical 3D simulation, a combined 2D simulation, a simplified analytical solution and a detailed semi-analytical solution with the aim of demonstrating the general applicability of them as well as commonalities and differences. Moreover, a parametric study was carried out with the investigated approaches in order to assess the dependence of the prediction quality of the various approaches on changing conditions.

2. Demonstration example

The demonstration example is shown in **Fig. 1**. It represents a through structure for the entrance of an under- pass of a road with a concrete strength class of C35/45. The focus of the demonstration example is set on the quantification of the hardening-induced stressing of the wall due to external restraining of the foundation. The long-term development of the restraint stresses in the wall due to superposition with any imposed deformation during service life, however, goes beyond the scope of this paper and is therefore not directly investigated in the demonstration example. Only the effect of surface drying in the rather thick wall is indirectly considered by the

specific way of analysing the results, see section 3.3 (2). Further information on the superposition of hardening-induced restraint stresses with restraint stresses due to imposed deformation during service life can be found in BAW Bulletin (2019) and the work of Jędrzejewska *et al.* (2018).

The investigated wall has a thickness of 0.8 m, a height of 4.0 m and a length of 12.0 m (L/H-ratio of 3.0). This wall will be directly casted on an already hardened slab of the same length but with a thickness of 1.0 m and a width of 20 m, which lays on homogenous sandy ground with a vertical bedding stiffness of 10^4 kN/m³.

It shall be assumed that the wall will be poured with a

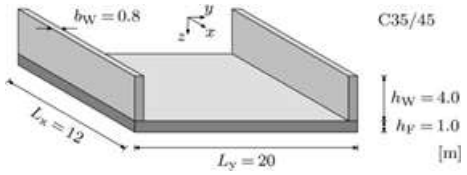

Fig. 1 Dimensions of the demonstration example.

fresh concrete temperature of 25°C, whereby the ambient temperature can be considered as constant with 20°C. The formwork material is plywood with a thickness of 2 cm and the wall will be kept in formwork for 7 days. The top surface of the wall will be covered during the first 7 days with a foil.

Necessary information regarding the behaviour of the concrete during hydration is available by a suitable data set containing measurements on the heat release, the evolution of strength and elastic modulus as well as autogenous shrinkage. The summary of these measure- ments together with the calibration of the material model are presented in section 3.2.

3. Thermomechanical 3D-FEM simulation

3.1 Geometrical idealization

The thermomechanical 3D-FEM simulation was carried out using the FE software SOFiSTiK. The volumetric calculation model was created with volume elements for the wall, the slab and a representative ground body, whereby symmetry was used in longitudinal and lateral direction. For the simulation of temperatures, all free surfaces of the calculation model (except the symmetry planes) were covered with surface elements which were used to simulate the heat transfer with the ambient environment. At the bottom of the slab, realistic temperature conditions were provided by the heat exchange with the representative ground body. For the subsequent simulation of stresses, the model was supported in longitudinal and lateral direction by the symmetry conditions. In vertical direction, however, the ground body was switched off during the stress simulation and the model was bedded on bi-linear bedding springs, which fail in tension. The calculation model is shown in **Fig. 2**.

The bi-linear bedding condition is needed to simulate the effect of a possible uplift of the model due to the eccentric restraining of the deformation behaviour of the wall. This is particularly important, since this activates the self-weight of the uplifting part of the model which

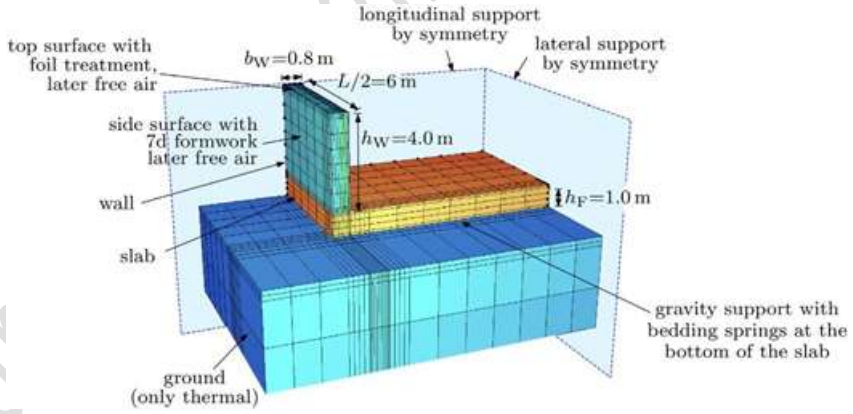

Fig. 2 Geometrical idealization.

causes in turn an additional outer moment acting on the whole cross section of wall and foundation slab. **Figure 3** exemplifies this effect schematically with the deformation figure as well as the bedding reaction in the two limit cases of maximum wall expansion at the temperature maximum and maximum shortening at the temperature equalization. Further information on this effect can be found in (Schlicke 2014; Schlicke *et al.* 2014).

In the present model, the bedding stiffness was defined with a compression stiffness of 10^6 kN/m³, whereby the bedding springs fail as soon as tension occurs. Contrarily to the given stiffness in compression of 10^4 kN/m³ in the specification of the example, a significantly higher value was regarded in the simulation in order to obtain conservative values for the self-weight activation. In reality, the self-weight activation due to uplift is partly reduced by the elastic bedding on the soil. However, the simulation of this favourable effect requires very good knowledge about the ground properties, which is usually not available. By using 10^6 kN/m³ in the present case, the maximum possible self-weight activation is simulated, whereby any favourable effect of a possible subsidence cavity was excluded on the safe side.

In horizontal direction, however, any possible restraining effect of the soil was neglected, since this effect is insignificant due to a substantially higher axial stiffness of the restraining slab compared to the axial stiffness of the activated soil body.

The material behaviour of the hardening wall was implemented time discretely with respect to the changing properties during hydration. This material behaviour was also implemented for each element independently in order to regard the different temperature and hardening histories within the cross section of the wall. On the contrary, the material behaviour of the foundation slab and the ground was set as constant over the simulation time.

3.2 Material model for hardening concrete

The thermomechanical 3D FEM solution requires a time-discrete material model with respect to the evolution of thermal and mechanical material properties throughout the hydration. For the simulation on structural level, this refers primarily to the release of heat of hydration, the evolution of stiffness and the occurrence of autogenous shrinkage. Another important material property of hardening concrete is its viscoelasticity, which depends both on the advancement of hydration and the stress history. All these evolutions need to be coupled in time and with respect to the maturity of the concrete, whereby the effect of maturity describes the dependence of the speed of hydration on the actual temperature of the concrete during the hydration process. A fundamental overview on this complex behaviour is given in (Fairbairn and Azenha 2018).

The present thermomechanical 3D FEM model contains a composition of different models for the description of the particular material properties, which were implemented for each element independently. The coupling was made on basis of the effective concrete age in each element, which serves as a state parameter to control the evolutions of the single properties. The viscoelastic behaviour was implemented by a specifically developed algorithm, which works for each element separately. In detail, this algorithm records the stress history of the simulation in each element, determines from this the occurring viscoelastic strains in the actual time step according to the creep curves of EN 1992-1-1 (2011) and imposes them in the actual time step. In phases with increasing stressing, this algorithm works with strict superposition in accordance with the superposition prin-

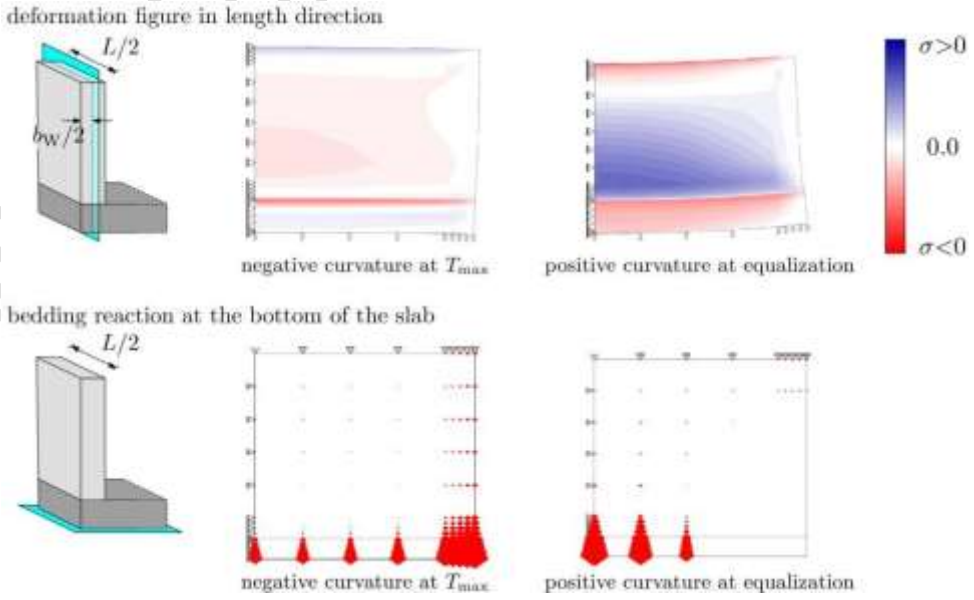

Fig. 3 Quantitative illustration of the effect of uplift due to eccentric restraining of the wall.

ciple of Boltzmann. In phases of decreasing stressing, however, the algorithm abolishes the superposition and reduces instead the viscoelastic potential of the prior stress changes according to the unloading. Further details on its functionality and verification are given in (Schlicke and Tue 2010, 2012, 2013; Schlicke 2014; Heinrich 2018; Jędrzejewska *et al*. 2018).

Figure 4a) shows the application of the applied models for the stress-independent properties in the present analysis. All other stress-independent parameters needed in the calculation were considered as constant over the time, even if they may show variations throughout hydration. These variations are assumed to be negligible from the structural perspective. Besides, **Fig. 4b)** illustrates the procedure for the simulation of viscoelastic effects on basis of creep strain increments. In the simulation, any stress change in each time step becomes an own creep curve according to the age of concrete at this time step. And all the occurring creep curves throughout time were collected, analysed for each new time step (change of creep coefficient in the time step multiplied with creep-effective strain) and regarded as additionally imposed deformation in the respective time step.

3.3 Results of the thermomechanical 3DFEM simulation

(1) Temperature and stress history

The results of the thermomechanical simulation are presented in **Fig. 5** for the decisive centre section of the wall. It shows the temporal evolution of temperatures in selected nodes and the temperature field at maximum temperature as well as the temporal evolution of longitudinal stresses in selected nodes and the stress field at temperature equalization.

(2) Analysis of the stress distribution

As expected, temperatures and stresses are strongly non-uniformly distributed over the cross section and over time. The main reason is the transient condition of the temperature field which causes pronounced non-uniform self-equilibrating stresses, hereinafter referred to as eigenstresses. Besides these eigenstresses, the stress field contains also stresses resulting from stress resultants (restraint force and restraint moment) which are in equilibrium with a restraint force and a restraint moment in the foundation as well as an outer moment due to activated self-weight of the structure.

The occurrence and opening of separating cracks in the wall are predominantly related to the stresses due to restraint force and restraint moment. Eigenstresses, however, are self-equilibrated in the cross section and cause in the first place merely surface cracks or locally restricted incipient cracks in the interior of the cross section, see (Schlicke and Tue 2014; Schlicke 2014; ÖBV Bulletin 2018). Of course, eigenstresses are expected to have a positive influence on the reduction of the cracking force, and thus their presence is taken into account for a reduction of the required minimum reinforcement for crack width control, see e.g. the regulations in EN 1992-1-1 (2011) or Bamforth (2017). But this should not be misinterpreted as a possibility to reduce the required minimum reinforcement by a planned

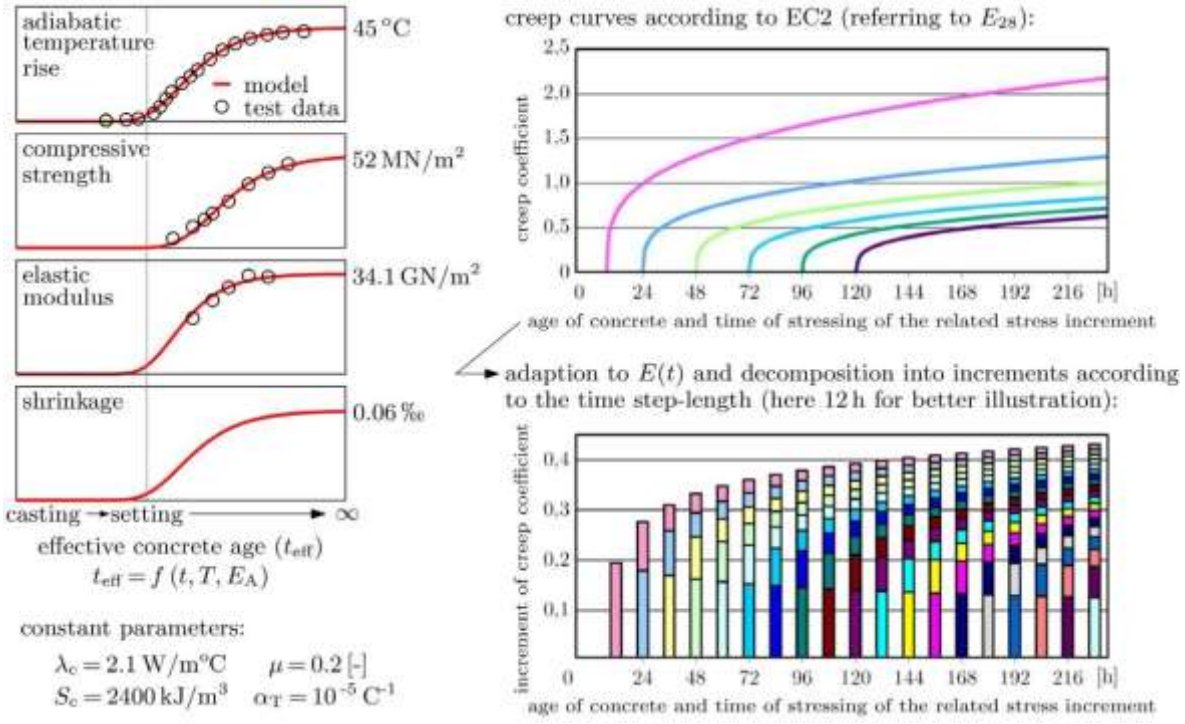

a) stress-independent properties b) incremental procedure for simulation of stress-dependent properties

Fig. 4 Relevant material behaviour of hardening concrete and their modelling for this study.

increase of eigenstresses. Aiming at durable structures, it is important to limit eigenstresses as much as possible in order to avoid surface cracking. And in view of the risk of separating cracks, eigenstresses can even have an obscuring effect, since they are usually reducing the maximum tensile stresses resulting from the stress resultants, as explained in (Schlicke and Tue 2014; Schlicke 2014; ÖBV Bulletin 2018). **Figure 6** exemplifies this effect with the stress distribution of the demonstration example at time of maximum tensile stresses due to stress resultants.

The stress field without eigenstresses was derived by integration of the stress field from the 3D FEM simulation. It should be noted, that this procedure removes also the non-linear parts of the stress distribution which arise from the membrane effect of the wall. Thus, the resulting stress distribution is plane, whereas other solutions could lead to a slightly curved course of stresses over the height of the wall.

In any case, **Fig. 6** is a suitable example to demonstrate the above-mentioned effect, that the absolute tensile stress maximum in the cross section can even be higher without eigenstresses. At the time of maximum tensile stresses due to stress resultants, which is usually at the time of temperature equalization, eigenstresses show compression at the surface and tension in the interior. The reason is that the hydration heat leads at first to a higher warming in the interior, as shown in **Fig. 5a**), which causes in turn a higher cooling potential in the interior. This leads to a prestressing of the surface zone, which reduces the tensile stress maximum due to restraint force and restraint moment, which is always at the bottom of the wall.

Nevertheless, this favourable prestressing of the surface zone due to thermal eigenstresses could later be reduced by drying of the surface zone. Aiming at the assessment of separating cracks on the safe side, it is therefore recommended to remove the eigenstresses from the stress field.

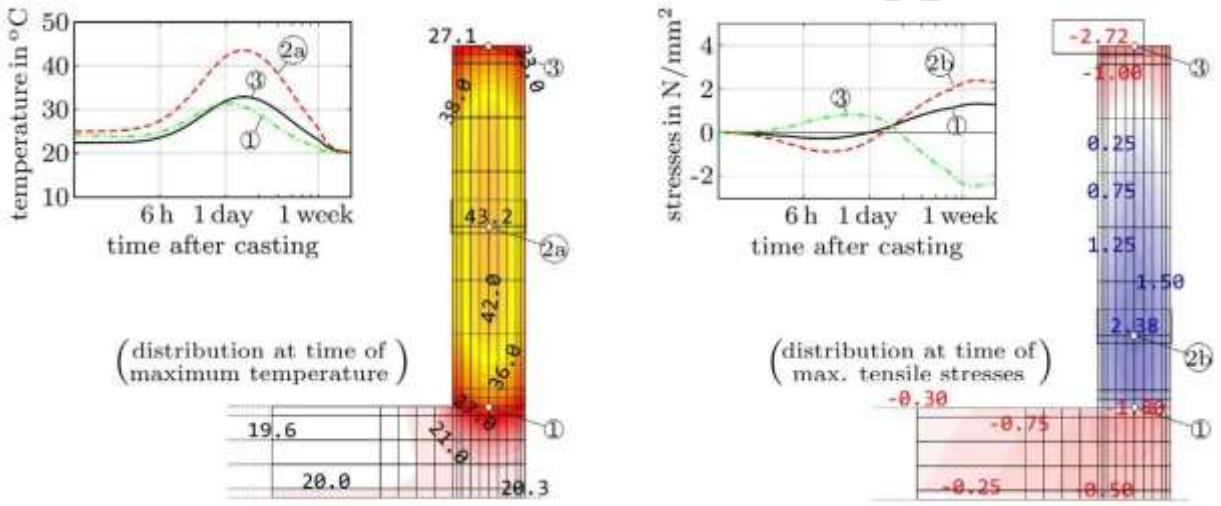

a) temperatures in °C b) stresses in N/mm²

Fig. 5 Results of a 3D FEM simulation: temporal course in selected points and cross-sectional distribution in the centre section.

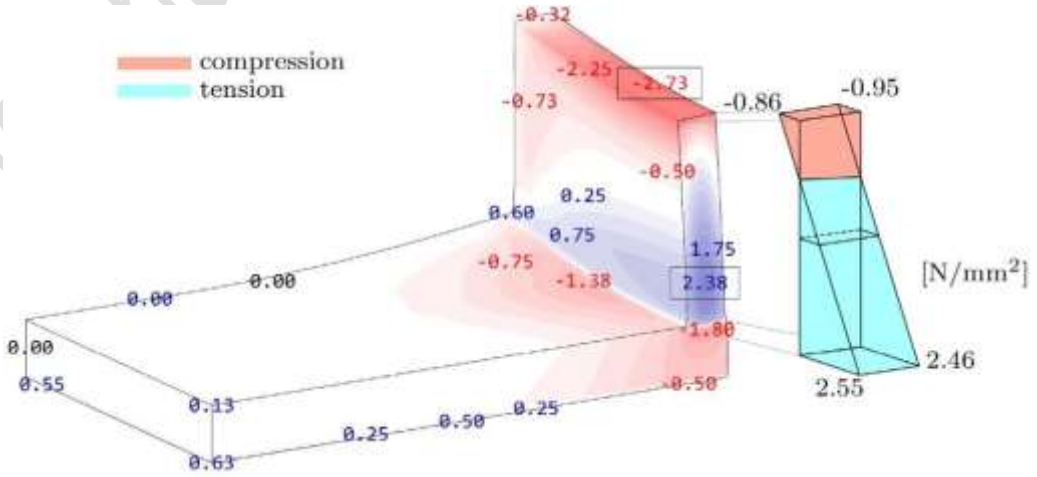

Fig. 6 Analysis of cross-sectional distribution of stresses with regard to stresses due to stress resultants and self-equilibrated eigenstresses.

4. Calculation with 2D-FEM models

In general, 2D FEM models enable two different solutions: (i) thermomechanical simulation of the temperature field in a cross section and determining the corresponding stress field for a given restraining condition of the cross section; and (ii) idealization of the system in length direction and determining the stress distribution over the height of the wall for a given imposed deformation. Of course, both approaches can be combined as exemplified for the demonstration example in subsection 4.1, however, such a combined solution does not implicitly include the eigenstresses due to the nonlinear part in the temperature field.

Besides, the finally determined stress distribution over the height of the wall is significantly influenced by a number of fundamental modelling assumptions. This refers to the different boundary conditions illustrated in **Fig. 7**, namely the axial restraining condition at the bottom of the wall (fully or partially restrained) as well as the restraining condition of the uplift (fully or partially restrained according to the self-weight activation).

The significance of these boundary conditions is illustrated in **Fig. 8** by a comparison of the degrees of restraint over the height of the wall for the cross-sectional dimensions of the demonstration example in **Fig. 1**, but different *L*/*H*-ratios. Due to the limitation, that the 2D model assumes a constant stress distribution over the width, the width of the foundation was taken into account with an effective width according to the simplified recommendation in section 5.1. This gives for the considered *L*/*H*-ratios of 2, 3 and 6 an effective width of the foundation of $b_{F,eff}$ = 4.8, 6.8 and 8.8 m.

In order to obtain realistic results, the partial restraining at the wall bottom should be taken into account. But it should be noted that a simple reduction of the degree of restraint over the height on basis of the axial stiffness ratio, as proposed by ACI (2007) or Bamforth (2017), can lead to unsafe results for shorter walls with a comparable small self-weight activation, see (Schlicke *et al*. 2018).

Besides, it should be noted that also the cases with full bottom restraint can show smaller degrees of restraint at the wall bottom than 100%. This is caused by the occurrence of lateral stresses when considering the Poisson's ratio for uncracked concrete and it is increasingly pronounced for shorter *L*/*H*-ratios. Further details and a comprehensive discussion on the significance of all these effects can also be found in (Schlicke *et al*. 2018).

4.1 Results for the demonstration example using combined 2D FEM

(1) Cross-sectional analysis of the temperature and stress field

In the first step, the two dimensions of the calculation model were used to perform a cross-sectional analysis of the temperature and stress field in the wall. For tem-

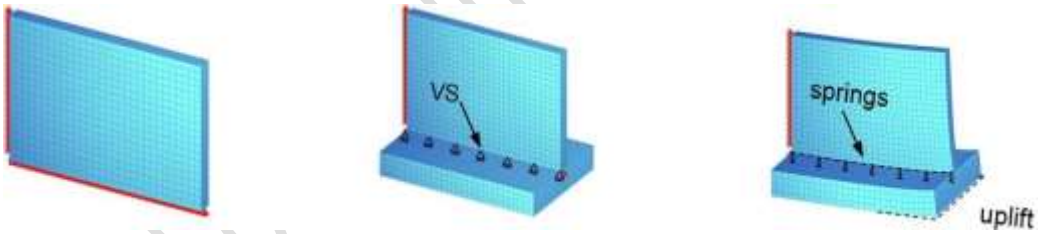

a) full bottom-restraint b) partial axial restraint but full restraint of uplift c) partial axial restraint and partial restraint of uplift

Fig. 7 Different approaches for 2D FEM analysis in length direction.

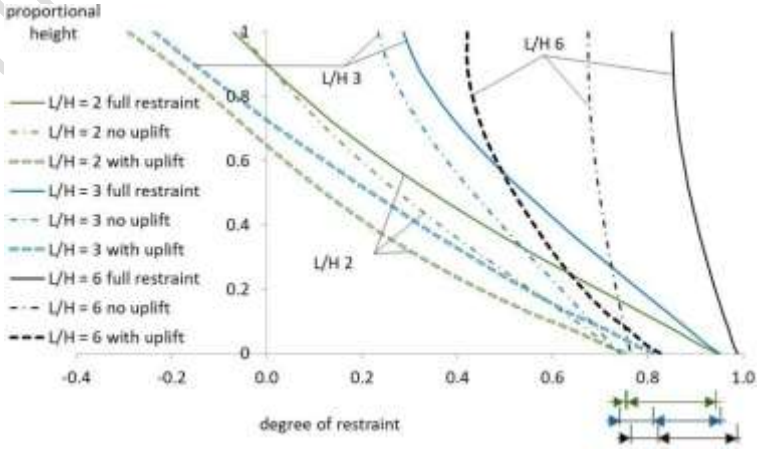

Fig. 8 Influence of different restraining conditions on the degree of restraint (full versus partial restraining of axial deformations at the bottom and uplift due to self-weight activation).

peratures, such approach leads to a similar temperature history and temperature distribution as determined with a thermomechanical 3D FEM model for the centre section given in **Fig. 5a**). On the contrary, the stress history and stress distribution will differentiate significantly from the 3D FEM results since it is not trivial to consider the partial restraining condition at the wall bottom as well as over the length direction due to partial uplift appropriately. Only limit cases such as full restraint (max. restraint forces), partial restraint in axial direction but full rotational restraint (representative for very long walls with no uplift near the centre section) or no axial restraint but plane cross section (only eigenstresses) could be easily simulated. **Figure 9** shows exemplarily the theoretical stress field for the condition of full restraint. Furthermore, this stress field was analysed and separated into its specific parts by integration, which leads to the given values for uniformly distributed stresses in the cross section (axial restraint), linearly distributed stresses over height and width (bending restraint) and remaining non-linearly distributed self-equilibrated stresses (eigenstresses).

(2) Analysis of the stress distribution over the height with a system in length direction

As stated above, the effect of the partial restraining conditions due to uplift of the wall requires a second analysis with a 2D system for the length direction. Hereby, eigenstresses cannot be regarded since the model assumes constant stresses over the width of the wall. Besides, the model assumes a symmetric location of the wall on the foundation. In view of the simulated restraining condition, this causes a small increase of restraint stresses compared to a solution with an asymmetric location, which was neglected for the benefit of a simple solution.

Overall, the deformation to be imposed in the system in length direction can be derived from the stresses given in **Fig. 9**. In general, this deformation to be imposed depends only on the stress resultants (axial and bending restraint), since eigenstresses are self-equilibrated within the cross section. Thus, the deformation to be imposed depends in the present case solely on the axial stressing σ_N. With respect to the elastic modulus in the model they can be determined with $\otimes\varepsilon_{eq} = -\sigma_N / E_c = -3.57 / 34.100 = -0.105‰$. From engineering perspective, this equivalent imposed deformation represents the temporal effects of stiffness evolution and creep with acceptable accuracy. **Figure 10** shows the result of such analysis in length direction, whereby the width of the foundation was again taken into account with an effective width (here: $b_{F,eff} = 6.8$ m for $L/H = 3$).

Overall, the obtained results of the combined 2D FEM solution show a good agreement with the results of the thermomechanical 3D FEM simulation. One criticism of the herewith presented 2D FEM solution is the fact, that the stiffness and the self-weight of the foundation is always activated over the whole width. Therefore, the appropriate definition of the effective width of the foundation is of high importance. Another opportunity is the idealization of the foundation as plate with horizontally arranged 2D elements, however, this solution is computationally demanding due to an irregular areal uplift. Besides, the stresses in the slab can be falsified which is usually of minor importance.

5. Calculations with analytical and semi-analytical approaches

In contrast to the presented numerical modelling, which can be very powerful and illustrative, analytical and semi-analytical approaches can provide very practicable and efficient solutions. Furthermore, analytical and semi-analytical approaches express explicitly the influence of individual system parameters and their cross-dependencies on the result.

In the following, two well-established analytical and

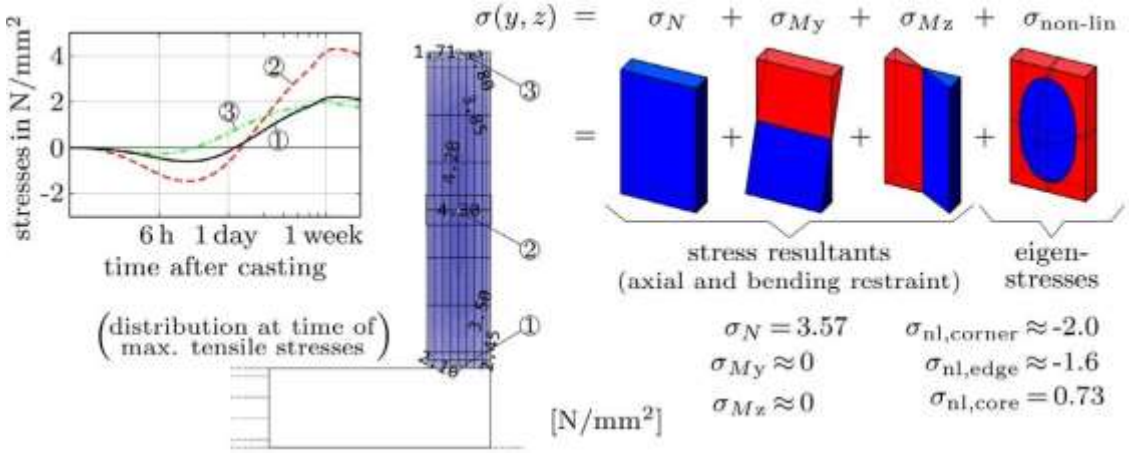

a) stress field for full axial restraint $\sigma(y,z)$ b) specific parts of the stress field

Fig. 9 Theoretical stresses in the centre section of the demonstration example determined with thermomechanical 2D FEM analysis for the condition of full restraint in axial direction

semi-analytical solutions were presented representatively. Other solutions can be found in the literature which are not discussed in this contribution. Further information is given in (Fairbairn and Azenha 2018).

5.1 Simplified calculation on basis of equilibrium and compatibility (TU Graz solution)

One possibility for stress calculation in walls is the simplified analytical solution proposed by Schlicke (2014). Aiming at a user-friendly and robust solution for practical application, this analytical approach was derived by only two fundamental conditions: (i) evenness of the cross section, and (ii) activation of self-weight according to the curvatures of the cross-sections along the member length. This provides a transparent solution for simple systems, however, further influences such as nonlinear effects in high walls or slip failure in the casting joint, are deliberately neglected. Nowadays, this approach was prepared for practical application in BAW Bulletin (2011), BAW Bulletin (2019) and ÖBV Bulletin (2018). The whole procedure is illustrated in **Fig. 11**.

The first condition can be satisfied by equilibrium and compatibility. For the equilibrium of restraint forces it reads:

$$N_W = -N_F \quad \text{and} \quad M_W + M_F = N_W \cdot y_1 \tag{1}$$

where:

- N_W, M_W inner normal force and inner moment acting on the cross section of the wall
- N_F, M_F inner normal force and inner moment acting on the cross section of the foundation
- y_1 inner leveler arm ($y_1 = (h_W + h_F)/2$)

And for the compatibility of strains it reads:

$$\kappa_W = \kappa_F \text{ and } \varepsilon_{W,F} = \varepsilon_{F,F} \tag{2}$$

where:

- κ_W, κ_F curvature of the cross sections of wall and foundation
- $\varepsilon_{F,F}$ strain in the centere of the cross section of the foundation
- $\varepsilon_{W,F}$ strain of the cross section of the wall extrapolated to the centre of the cross section of the foundation

Equalizing Eq. (1) and Eq. (2) the inner forces acting in the cross section of the wall can be determined on basis of the equivalent imposed deformation $\otimes\varepsilon_{eq}$ with:

$$N_W = -\otimes\varepsilon_{eq} \left(\frac{1}{E_F A_F} + \frac{1}{E_W A_W + \frac{y_1^2}{E_F I_F + E_W I_W}} \right)^{-1} \tag{3}$$

$$M_W = N_W \cdot y_1 \cdot \frac{1}{1 + \frac{E_F I_F}{E_W I_W}} \tag{4}$$

where:

- $E_F A_F$ axial stiffness of the foundation
- $E_W A_W$ axial stiffness of the wall
- $E_F I_F$ bending stiffness of the foundation
- $E_W I_W$ bending stiffness of the wall

The condition of the equilibrium between internal forces of wall and foundation is an even cross section, however, this cross section has a curvature due to the eccentric restraint. Added up along the member length

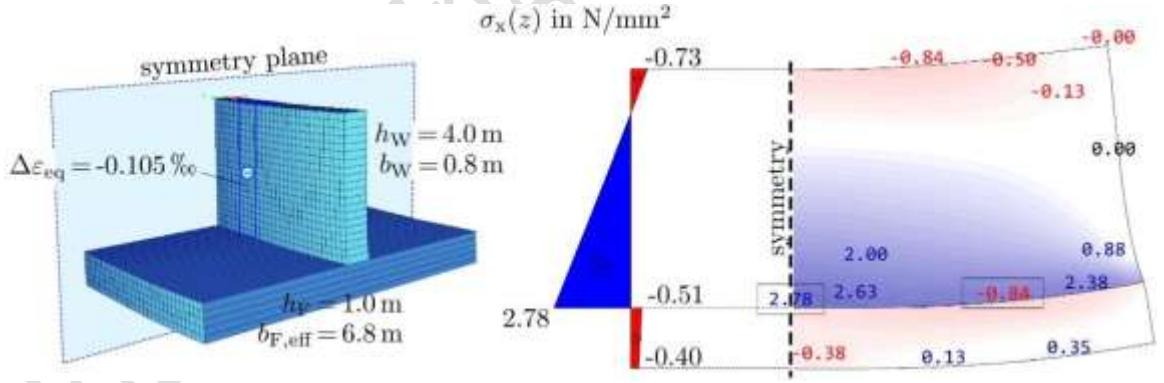

Fig. 10 Resulting stresses in length direction of the demonstration example determined with 2D FEM and regard to partial restraint in axial direction and uplift.

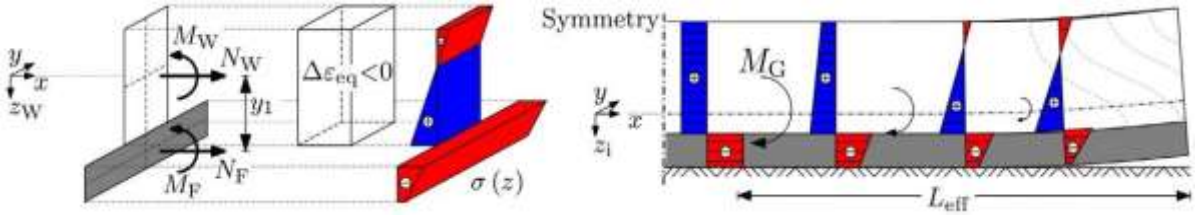

a) inner restraint forces and stress distribution due to cross section compatibility

b) resulting stress distribution with regard of an outer bending moment due to uplift of the whole system

Fig. 11 Simplified stress distribution in bottom-restrained walls acc. to Schlicke (201

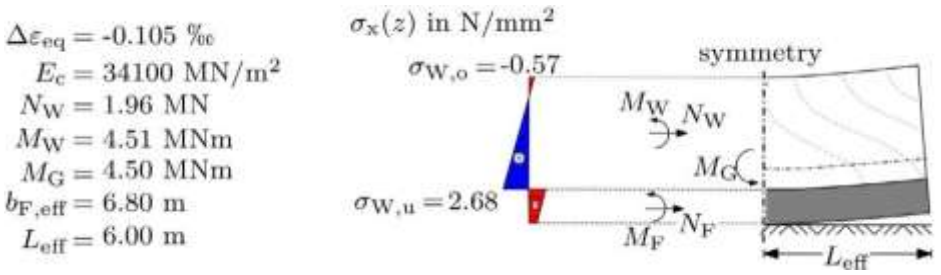

Fig. 12 Stress distribution of the demonstration example determined with the solution acc. to Schlicke (2014).

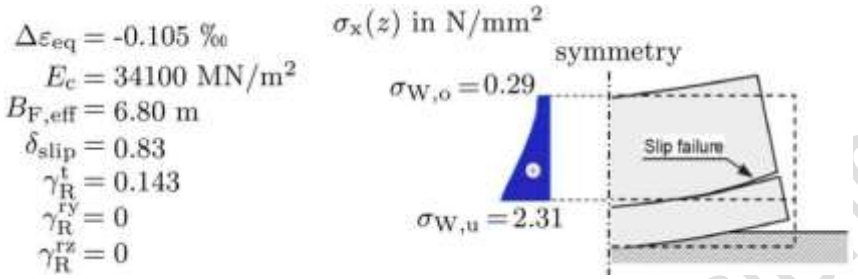

Fig. 13 Stress distribution of the demonstration example determined with the solution acc. to Nilsson (2003).

6. Calculation on basis of current regulations

(1) Eurocode 2 – Part 3

The approach in EN 1992-3 (2006) offers a set of empirical restraint factors that have been derived for typical geometries of concrete pours. The resulting stresses are determined from the degrees of external restraint to axial R_N and flexural movements R_M. For walls on foundations, the approach recommends a full flexural restraint $R_M = 1$ and a single value of axial restraint $R_N = 0.5$ at the bottom joint. Besides, the given values in EN 1992-3 (2006) account implicitly for the reduction of restraint due to creep with a recommended value of 0.65, see eg. (Zych 2018).

Figure 14 shows the solution of EN 1992-3 (2006) and gives the result of applying these restraint factors for the demonstration example and the equivalent deformation to be imposed according to section 4.1 (1) Since this equivalent deformation includes already the effect of a reduction of restraint stresses due to creep, the external restraint at the bottom is here taken as $R_N = 0.5/0.65$. The given values in brackets refer to $R_N = 0.5$.

(2) ACI

The approach in ACI (2007) provides a two-step procedure for estimating the degree of restraint over the height of the wall. At first, the course of the degree of restraint over the height of the wall can be taken from a chart with respect to the *L*/*H*-ratio (factor $K_R(z)$). This solution complies with the result of a shell model with complete axial and bending restraint at the bottom of the wall, which is shown in **Fig. 7a)**. And in a second step, it is recommended to reduce the course over the whole height of the wall by the degree of axial restraint according to the axial stiffnesses of wall and foundation (factor $K_F = [1 + A_W E_W / A_F E_F]^{-1}$). **Figure 15** shows the graph in ACI (2007) and gives the result of applying these restraint factors for the demonstration example with the equivalent deformation to be imposed according to section 4.1 (1) and $B_{F,eff} = 6.8$ m according section 5.1.

7. Parametric study

The prior study obtained an acceptable agreement between the results of the different methods, especially for the maximum tensile stresses at the bottom of the wall. With the following parametric study, the sensitivity of this agreement will be investigated. The focus will hereby set on the influences of three key parameters, namely the *L*/*H*-ratio, the bending stiffness of the foundation and the quantity of imposed deformations. The effective width of the foundation is hereby again considered according to the simplification in section 5.1 with $B_{F,eff} = 4.8, 6.8, 8.8, 10, 10, 10$ m for the *L*/*H*-ratios of 2, 3, 4, 6, 8 and 10.

The result analysis of the parametric study will be

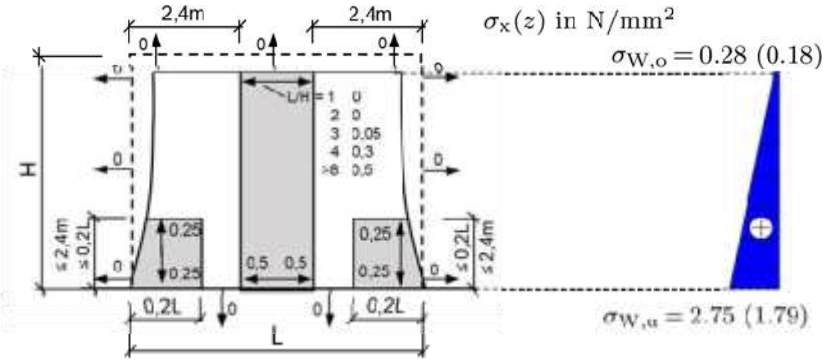

Fig. 14 Restraint factors RN acc. to EN 1992-3 (2006) and resulting stress for the demonstrations example.

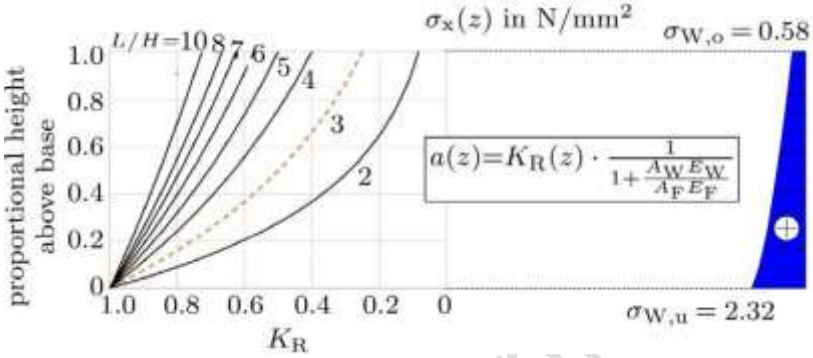

Fig. 15 Restraint factors R_N acc. to ACI (2007) and resulting stresses for the demonstration example.

based on a comparison of the resulting degrees of restraint. In the methods in which the degree of restraint is not explicitly determined (3D and 2D FEM analysis as well as analytical approaches of section 5.1 and 5.2) it will be determined by dividing the calculated stress with the theoretical stress of full restraint.

7.1 Influence of L/H on the degree of restraint

Figure 16 shows the degrees of restraint over the wall height for the cross-sectional dimensions of the demonstration example but with different *L/H*-ratios. It can be seen that the FEM solutions agree with each other very well over the whole range, whereas the analytical solutions (here labelled with TU Graz and Luleå) show qualitatively the same behaviour but with a stronger increase of the degree of restraint with increasing *L/H*. On the contrary, the solutions of current regulations (ACI and EC 2) indicate a significantly smaller increase of the degree of restraint over the height with increasing *L/H*.

7.2 Influence of the bending stiffness of the foundation on the degree of restraint

Figure 17 shows the results of an analysis with different cross-sectional dimensions with the primary focus to indicate the influence of the bending stiffness of the restraining foundation. The study was carried out with the 3D model, whereby the ratio of axial stiffnesses between wall and the foundation (A_W/A_F) was kept constant while the bending stiffness of the foundation was varied by the modification of its height (h_W/h_F). For example, a ratio of A_W/A_F = 0.33 and h_W/h_F = 4 represents the demonstration example, whereas the combination of A_W/A_F = 1 and h_W/h_F = 1 would refer to a wall which is cast on a foundation of the same dimensions as the wall itself.

As it will be shown later, these results depend also on the quantity of the imposed deformation. Therefore, it is explicitly mentioned that the results in **Fig. 17** refer to an imposed deformation of $\otimes\varepsilon_{eq} = -0.1‰$ and elastic moduli of $E = E = 30000$ MN/m². For a better illus-

tration, the results are given here only for the values of the degree of restraint at the bottom and the top of the

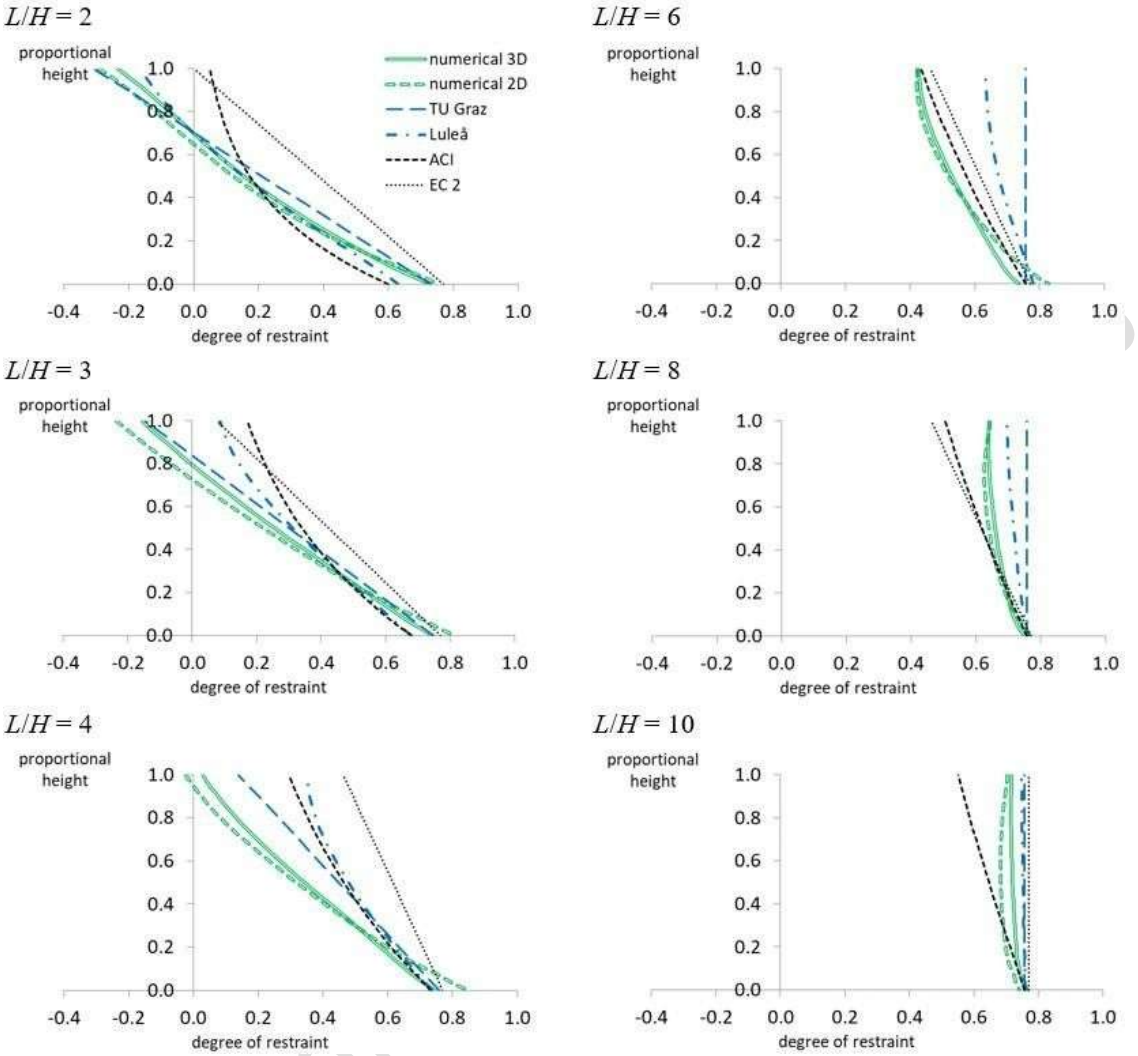

Fig. 16 Degree of restraint for the demonstration example acc. to different approaches.

wall.

The results indicate a recognisable influence of the well as the analytical solution of TU Graz. The study was carried out with the elastic moduli of bending stiffness, which can change the degree of re- straint by up to 25% over the investigated range. The reason for this behaviour is an interplay between the internal moments caused by eccentric restraint and the additional outer moment due to the self-weight activa- tion. As shown in the works of Schlicke (2014) or Schlicke *et al*. (2018), this interplay is also strongly affected by the location of the centre of gravity of the total cross section of wall and foundation. If this centre of gravity lies above the bottom of the wall, the self- weight activation causes beneficial compressive stresses at the bottom of the wall, which is more pronounced with increasing *L/H*. On the contrary, cases with a centre of gravity below the bottom of the wall show always increasing tensile stresses at the bottom of the wall with increasing *L/H*. This effect is implicitly considered in all solutions with a targeted consideration of the self-weight activation, e.g. FEM with uplift or analytical approaches of TU Graz and Luleå. On the contrary, the empirical approaches of the current regulations do not regard this effect appropriately.was varied in a range of □T □ □T □

$E = E = 30000\text{MN} / \text{m}^2$

7.3 Influence of the quantity of the imposed de- formation

Besides geometrical conditions, the degree of restraint depends also on the quantity of the imposed deforma- tion as long as the self-weight is not fully activated. **Figure 18** illustrates this effect with the results of a pa- rametric study on basis of the cross-sectional dimen- sions of the demonstration example using 3D FEM as $10^{-5} \cdot$ (–2.5 ... –20) °C This range represents equivalent temperatures to be imposed and covers common condi- tions in practice.

The results indicate a recognisable influence of the quantity of the imposed deformation, which is increas- ingly pronounced in shorter walls with rather small self- weight activation, e.g. for *L/H* = 3. The reason is that the

self-weight activation depends on the curvature due to eccentric restraint of the imposed deformation und thus, also on the quantity of the imposed deformation. This effect is implicitly considered in all solutions with a targeted consideration of the self-weight activation, e.g. FEM with uplift or analytical approaches of TU Graz and Luleå. On the contrary, the empirical approaches of the current regulations do not regard this effect appro- priately.

8. Discussion and conclusion

This contribution investigated the performance of dif- ferent concepts for determining restraint stresses in bot- tom-restrained walls. The investigated approaches range from advanced computational methods over analytical and semi-analytical solutions up to empirical ap- proaches, which can be found in several guidelines.

In the first part of the paper, these different concepts were all applied on the same demonstration example in order to assess and compare their applicability and accu-

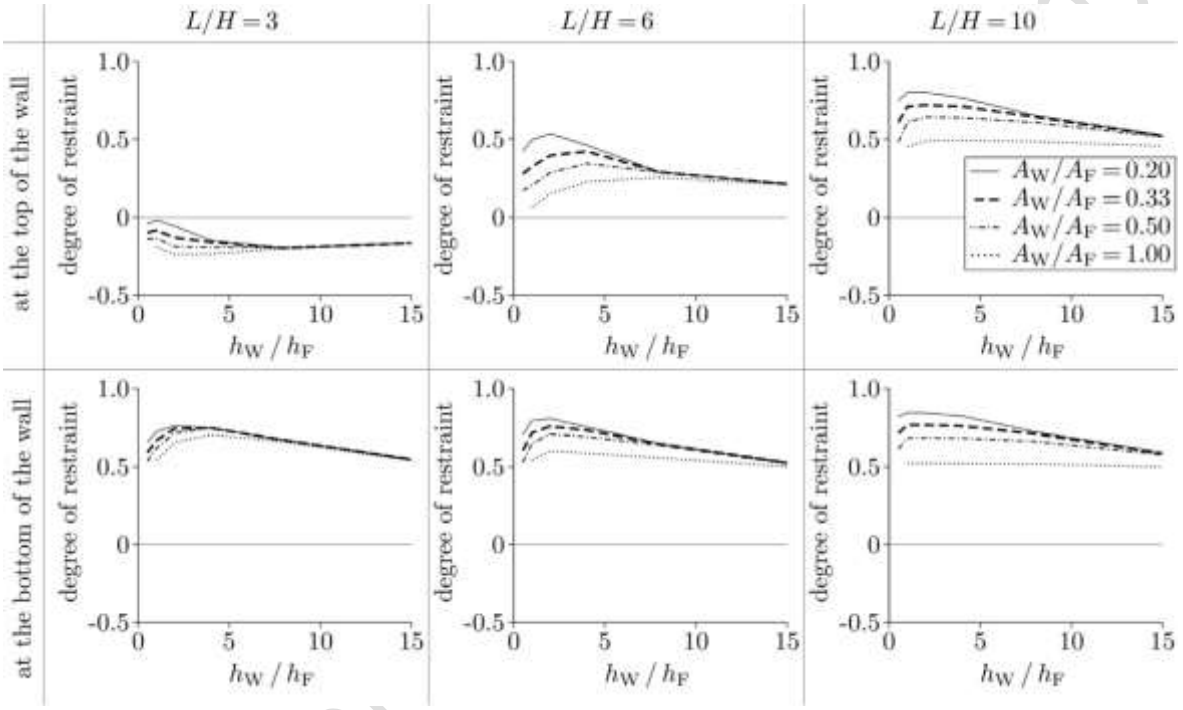

Fig. 17 Influence of the cross-sectional dimensions on the degree of restraint for different *L/H*-ratios according to 3D FEM simulations.

Table 1 Comparison of results for the demonstration example using different solutions.

Solution	$\sigma_{c,bottom}$ [N/mm²]	$\sigma_{c,top}$ [N/mm²]	deviation, bottom	deviation, top
thermomechanical 3D FEM	2.51	-0.91	-	-
combined 2D FEM	2.78	-0.73	+ 10 %	− 20 %
analytical solution TU Graz	2.68	-0.57	+ 7 %	− 37 %
Semi-analytical solution Luleå	2.31	0.29	− 8 %	change of sign
empirical regulation EC2-3	2.75	0.28	+ 10 %	
semi-empirical regulation of ACI	2.32	0.58	− 8 %	

racy.

For the purpose of a better comparison, the particular results of each method are listed in Tab. 1. It can be seen, that the study obtained a good agreement for the maxi- mum tensile stresses at the bottom of the wall with a deviation of less than ± 10%. Regarding the stresses at the top of the wall, the thermomechanical 3D FEM solu- tion indicates the highest compressive stresses, whereby the combined 2D FEM solution and the analytical solu- tion of TU Graz indicate also compressive stresses but significantly smaller (− 20% and − 37%), meanwhile the other solutions indicate even tensile stresses.

The stresses at the top of the wall depend greatly on the activated self-weight and therefore on the effective width of the foundation. This effective width was assumed in all solutions (except 3D) with the same value,which was derived from a simplified approach on basis of a stress diffusion angle (see section 5.1). On basis of the results it can be concluded, that this assumption was conservative for solutions with explicit consideration of self-weight activation, whereas solutions without ex- plicit consideration of self-weight activation lead to very conservative results in general.

In the second part of the paper, a parametric study was conducted in order to investigate the influence of different conditions and input parameters on the performance of the investigated methods. It was found, that the results deviate the most due to the effect of self-weight activation caused by uplift of the free corner of the wall. The computational methods as well as the analytical solutions regard this effect explicitly, whereas this is not pursued further in the tested approaches from the guidelines. The computational methods as well as the analytical solutions therefore show a plausible response to varying *L/H*-ratios, changing cross-sectional dimensions and ratios of bending stiffnesses and even to the quantity of the imposed deformation. As shown in the parametric study, these effects can influence thedegree of restraint to a large extent and should be seriously considered in structural design.

Overall, this contribution may serve as a decision guidance to choose the suitable solution for a specific design task as well as a basis for the discussion on possible disagreements between different solutions. Fur-

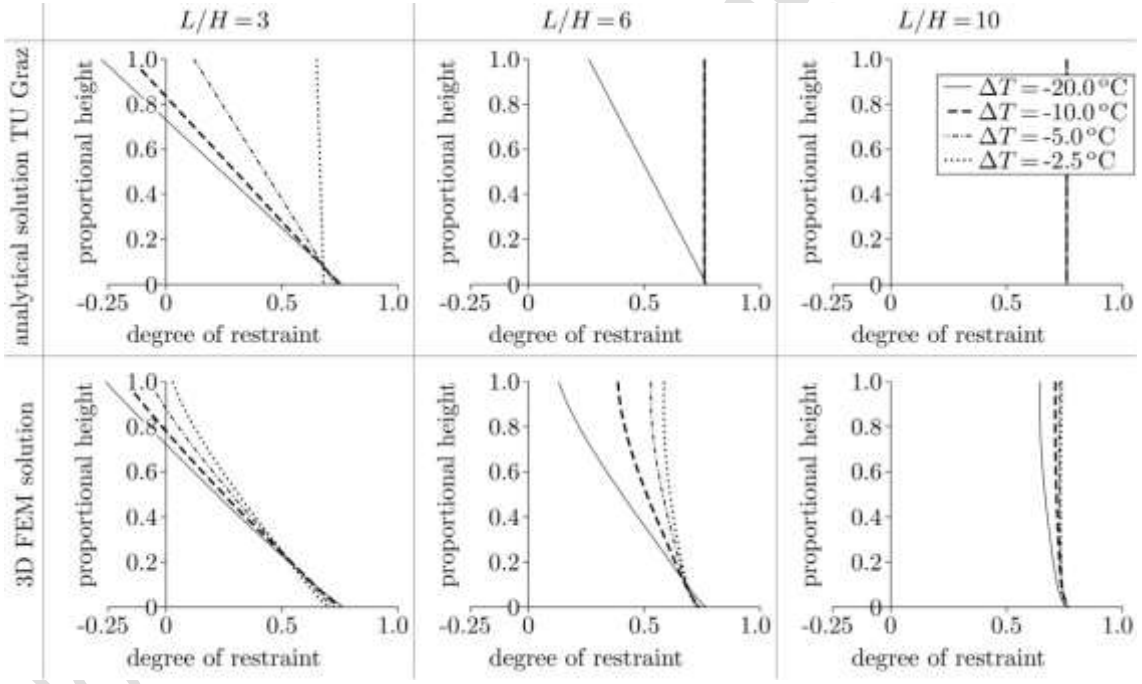

Fig. 18 Influence of the quantity of the imposed deformation on the degree of restraint for different *L/H*-ratios according to analytical solution and 3D FEM simulations.

thermore, it should be emphasised again, that the reliable assessment of cracking risk and crack width control requires the suitable consideration of all imposed de- formations, starting from hardening-induced stressing due to the cement hydration up to long-term behaviour throughout the whole service life of the structural mem- ber. The demonstration example focussed so far only on the determination of hardening induced stressing. Any negative influence of surface drying was solely regarded indirectly by neglecting the beneficial prestressing of the surface zone due to thermal eigenstresses. Of course, this assumption requires further verification. Next to this, the occurrence of additional stresses due to the variation of ambient temperatures and drying of the whole cross section needs to be determined. Internal interactions between wall and foundation due to ambi- ent temperatures and drying can be determined with the presented solutions, directly. Additional curvatures act- ing on the combined cross section of the wall and foun- dation, however, need to be determined with respect to the bending stiffness of the whole cross section. Further information is given in BAW Bulletin (2019) and Jędr- zejewska *et al*. (2018).

Acknowledgements

This contribution was completed with the support of COST Action TU1404 (STSM grant No. 34986) together with the support of the Scientific Grant Agency VEGA under the contract No. VEGA 1/0456/17.

References

- ACI, (2007). "*Report on thermal and volume change effects on cracking of mass concrete*." Farmington Hills: American Concrete Institute. ACI 207.2R-07.
- Bamforth, P. B., (2017). "*CIRIA C766: Control of cracking caused by restrained deformation in concrete*." London: CIRIA.
- BAW Bulletin, (2011). "*Crack width limitation for restraint stresses at early age in massive hydraulic structures*." Karlsruhe: Federal Waterways Engineering and Research Institute, Edition 2011. (in German)
- BAW Bulletin, (2019, in press). "*Crack width limitation for restraint stresses in massive hydraulic structures*." Karlsruhe: Federal Waterways Engineering and Research Institute, Edition 2019. (in German)
- COIN, (2011). "*Basis for and practical approaches to stress calculations and crack risk estimation in hardening concrete structures*." Oslo: Building and Infrastructure 2011, COIN Project report 31.
- EN 1992-1-1, (2011). "*Design of concrete structures, Part 1-1: General rules and rules for buildings*." Brussels: CEN.
- EN 1992-3, (2006). "*Design of concrete structures, Part 3: Liquid retaining and containment structures*" Brussels: CEN.
- Fairbairn, E. M. R. and Azenha, M., (2018). "*Thermal cracking of massive concrete structures. State of the art report of the RILEM TC 254-CMS*." 1st ed. Springer.
- Heinrich, P., (2018). "*Efficient consideration of viscoelastic properties for the determination of restraint stresses in restrained concrete members*." Thesis (PhD). Graz University of Technology. (in German)
- Jędrzejewska, A., Benboudjema, F., Lacarrière, L., Azenha, M., Schlicke, D., Stefano, D. P., Delaplace, A., Granja, J., Hájková, K., Heinrich, P. J., Sciumè, G., Strieder, E., Stierschneider, E., Šmilauer, V. and Troyan, V., (2018). "COST TU1404 benchmark on macroscopic modelling of concrete and concrete structures at early age: Proof-of-concept stage." *Construction and Building Materials*, 174, 173-189.
- JSCE, (2007). "*Guidelines for concrete, 15: Standard specifications for concrete structures. Design.*" Tokyo: Japan Society of Civil Engineers.
- Knoppik-Wróbel, A., (2015). "*Analysis of early-age thermal–shrinkage stresses in reinforced concrete walls.*" Thesis (PhD). Silesian University of Technology.
- Knoppik-Wróbel, A. and Klemczak, B., (2015). "Degree of restraint concept in analysis of early-age stresses in concrete walls." *Engineering Structures*, 102, 369-
- 386.
- Matiašková, L. and Šoltész, J., (2017). "Macroscopic calculation model for simulating early age behavior of concrete members." In: *Early Age Cracking and Serviceability in Cement-based Materials and Structures, Vol. 2,* Brussels 12-14 of September 2017.
- RILEM Publications, 695-701.
- Nilsson, M., (2003). "*Restraint factors and partial coefficients for crack risk analysis of early age concrete structures.*" Thesis (PhD). Lulea University of Technology.
- ÖBV Bulletin, (2018). "*Analytical design of watertight structures with optimized concrete.*" Vienna: Austrian society for construction technology. (in German)
- Schlicke, D., (2014). "*Minimum reinforcement for restrained concrete*." Thesis (PhD). Graz University of Technology. (in German)
- Schlicke, D. and Tue, N. V., (2010). "Measurement of thermal restraint in hardening mass concrete - a new approach exemplified by a thick foundation slab." In: *Proceedings of 6th Central European Congress on Concrete Engineering*, Marianske Lazne 30 September - 1 October 2010. CCC2010. 179-184.
- Schlicke, D. and Tue, N. V., (2012). "Approach for consideration of viscoelasticity in time step FEM based restraint analyses of hardening concrete." In: *Proceedings of 1st International Conference on Numerical Modeling Strategies for Sustainable Concrete*

Structures, Ais-en-Provence 29 May - 1 June, 53.

- Schlicke, D. and Tue, N. V., (2013). "Consideration of viscoelasticity in time step FEM-based restraint analyses of hardening concrete." *Journal of Modern*